Chapter 1
Superconducting Magnets for Accelerators

Alexander V. Zlobin and Daniel Schoerling

Abstract Superconducting magnets have enabled great progress and multiple fundamental discoveries in the field of high-energy physics. This chapter reviews the use of superconducting magnets in particle accelerators, introduces Nb_3Sn superconducting accelerator magnets, and describes their main challenges.

1.1 Circular Accelerators and Superconducting Magnets

Circular accelerators are the most important tool of modern high-energy physics (HEP) for investigating the largest mass and the smallest space scales. A key element of a circular accelerator is its magnet system (Wolski 2014). The magnet system is composed of large number of various magnets, mainly dipoles and quadrupoles, to guide and steer the particle beams. The main function of the majority of the magnets (the so-called arc magnets, which are periodically placed along a ring) is to keep the beam on a quasi-circular orbit and confine them in a relatively small and well-defined volume inside a vacuum pipe. Magnets are also used to transfer beams between accelerator rings in so-called transfer lines, to match beam parameters from the transfer line into the injection insertions or into extraction lines and beam dumps, to direct or separate beams for the accelerating radio frequency cavities, and to focus beams for collision at the interaction points where the experiments reside.

One of the most important parameters of colliders is the beam energy, as it determines the physics discovery potential. The energy E in GeV of relativistic particles with a charge q in units of the electron charge in a circular accelerator is limited by the strength of the bending dipole magnets B in Tesla and the machine radius r in meters

A. V. Zlobin (✉)
Fermi National Accelerator Laboratory (FNAL), Batavia, IL, USA
e-mail: zlobin@fnal.gov

D. Schoerling
CERN (European Organization for Nuclear Research), Meyrin, Genève, Switzerland
e-mail: Daniel.Schoerling@cern.ch

D. Schoerling, A. V. Zlobin (eds.), *Nb_3Sn Accelerator Magnets*, Particle Acceleration and Detection, https://doi.org/10.1007/978-3-030-16118-7_1

$$E \approx 0.3qBr.$$

Thus, high magnetic fields are an efficient way towards higher energy machines for hadron and ion collisions.

The value of the magnetic field in a circular accelerator needs to be synchronized with the beam energy. It is achieved by using electromagnets that allow the field strength to be varied by changing the electric current in the coil. The maximum field of traditional electromagnets with copper or aluminum coils is limited, however, by Joule heating, which limits the current density in a magnet coil typically to ~10 A/mm^2.

In 1911, the Dutch physicist H. Kamerlingh-Onnes discovered the phenomenon of superconductivity—the vanishing of electrical resistance in some metals at very low (<10 K) temperatures (Wilson 2012). This discovery inspired him 2 years later to propose a 100,000 Gauss (10 T) solenoid based on a superconducting coil cooled with liquid helium. He believed that superconductivity would allow the current in a coil to be increased and, thus, a larger magnetic field to be generated. Yet, it took more than 50 years of hard work to realize this dream in practice.

The design and construction of superconducting magnets have become possible only after the discovery and development in the early 1960s of technical superconductors. Technical superconductors are defined as a class of superconducting materials that provide high current densities in the presence of high magnetic fields.

Earlier attempts to use technical superconductors in superconducting magnets failed due to premature magnet transitions to the normal state, called quenches. These quenches were caused by the abrupt movement of magnetic flux inside a superconductor, the so-called flux jump effect. The analysis of flux jumps led to the development of stability criteria for technical superconductors (Wilson, 1983; Rogalla and Kes 2012). Stability of the superconducting state with respect to small field or temperature perturbations can be guaranteed only if the superconductor transverse size does not exceed a maximum value proportional to the material's specific heat, and inversely proportional to its critical current density. For example, for a Nb-Ti superconductor at 5 T and 4.2 K the maximum filament size has to be smaller than 50 μm.

The other main concern was protection of the superconductor in the case of a quench. All superconductors in the normal state have high resistivity. In the case of a quench they are likely to be damaged by Joule heating due to the high current density they carry, if no adequate measures for protection are taken. To minimize heating after a quench, a superconductor should therefore be surrounded by a normal conductor with a low resistance.

The two abovementioned conditions (stability and protection) have led to the concept of composite superconductors, in which small superconducting filaments are embedded in a normal conducting matrix with low resistance and large thermal diffusivity. The matrix decreases the Joule heating when the superconductor becomes normal, conducts the heat away from the surface of the superconducting filaments thanks to its high thermal conductivity, and absorbs a substantial fraction of heat due to its high specific heat. To provide stability of a composite

superconductor to flux jumps and reduce the eddy currents induced by varying external magnetic fields, the superconducting filaments are twisted along the conductor axis. Flux jumps not only limit the size of the filaments, but also the size of the multifilament composite wire due to self-field instabilities related to the non-uniform distribution of transport current inside the wire. For example, for a Nb-Ti composite wire at 5 T and 4.2 K, the maximum diameter is limited to ~2 mm.

A composite superconductor placed in a varying magnetic field becomes magnetized with two components: one is related to persistent currents in superconducting filaments, and the second is caused by coupling eddy currents between filaments. Both components are diamagnetic in an increasing field and paramagnetic in a decreasing field. The hysteretic behavior of wire magnetization leads to energy dissipation, also called alternating current (AC) losses. Likewise the magnetization, the AC loss power in a composite superconductor has two main components: one is related to persistent currents in superconducting filaments and the other one to coupling eddy currents in composite wires. The magnetization of composite wires plays an important role in superconducting accelerator magnets, which have demanding requirements on field uniformity. The AC losses are important for cryogenic cooling of superconducting coils during magnet operation and quench, and contribute to the heat load on a magnet's cooling system.

The critical current density J_c is a key parameter, which controls the current carrying capability, stability, magnetization, and AC losses of technical superconductors and, thus, the performance of superconducting magnets. As the resistive transition from superconducting to the normal conducting state in a composite superconductor is smooth, the definition of J_c is not straightforward (Warnes and Larbalestier 1987). The most commonly used criterion at the present time, for superconducting accelerator magnets in particular, defines J_c at the resistivity of $10^{-14}\ \Omega\,\mathrm{m}$.

Important features of practical materials for superconducting magnets include not only the appropriate combination of critical parameters, but also their reproducibility in long lengths, compliance with mass production, and affordable cost.

Large accelerator magnets use large, high-current cables to reduce the magnet's inductance, which is an important parameter for magnet protection during a quench. To achieve the required high current level, several strands are connected in parallel, and twisted or transposed in the axial direction (Wilson 1983). Multi-strand cables allow a reduction of the piece length requirement for wire manufacturing, the number of turns in a magnet coil, and also allow for current redistribution between strands in the case of a localized defect of some strands or quench. The Rutherford cable is the most widely used cable type in accelerator magnets (Gallagher-Daggit 1973). To adapt the cable design to the magnet design, it is produced with either a rectangular or a slightly keystoned cross-section. A Rutherford cable is composed of fully transposed twisted composite strands. Strand transposition reduces coupling losses and ensures uniform current distribution, also aided by the electrical contact between the strands. The cable critical current I_c is normally the sum of the strand's critical currents, which depend on wire degradation during cabling and current distribution in the cable cross-section. Due to strand coupling inside the cable, its magnetization and AC losses have additional eddy current components controlled by the interstrand resistance and the cable twist pitch.

1.2 Accelerator Magnet Design and Operation

1.2.1 Magnetic Design

The desired magnetic field in superconducting magnets is produced by a current I in a coil and is calculated using the Biot–Savart law

$$\vec{B} = \frac{\mu_0}{4\Pi}\int_C \frac{I\mathrm{d}\vec{l} \times \vec{r}}{r^3},$$

where $I\mathrm{d}l$ is a current element and r is the radius vector from the current element to the field point. The total field in a given point of a magnet is obtained by integrating the current elements over the coil volume.

A perfect dipole field can be generated by two infinite slabs, by two intersecting ellipses (cylinders) with uniform and equal currents of opposite direction, or by a cylinder with a cos-theta current density distribution (Fig. 1.1) (Brechna 1973). The field strength B in the dipole aperture is defined as

$$B \sim J(B)w,$$

where w is the slab or cylinder thickness.

To mimic the ideal current configurations, they are approximated with a number of cables arranged in blocks and separated by wedges (Russenschuck 2010). The block positions and cross-sections are optimized to approach the ideal coil cross-section and achieve the required field quality. In practice, in line with the three different types of dipolar configurations in Fig. 1.1, three coil types are used: block, shell, and cos-theta.

Coils of accelerator magnets are usually surrounded by an iron yoke, which serves as a return path for the magnetic flux and contributes to the magnet bore field. Three different classes of magnets can be identified based on the way in which the wanted field is achieved: (a) iron dominated or superferric magnets, in which the shape of iron poles determines the field pattern; (b) iron-free magnets, in which the field configuration is dominated by the coil shape; and (c) magnets, in which the field configuration is provided by both the coils and the iron yoke.

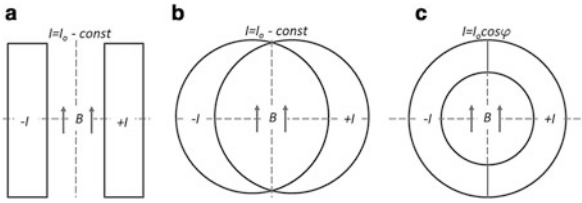

Fig. 1.1 Pure dipole configurations: (**a**) two infinite slabs; (**b**) intersecting ellipses; and (**c**) cylinder with cos-theta azimuthal current density distribution

1.2.2 Field Quality

Since real coils only approximate the ideal dipole cross-sections, the magnetic fields in accelerator magnets are not perfect. Excluding the coil ends, the magnetic field in the bore of long and slender accelerator magnets is two-dimensional and can be represented by the power series (Mess et al. 1996; Russenschuck 2010)

$$B_y + iB_x = B_1 \sum_{n=1}^{\infty} (b_n + ia_n) \left(\frac{x + iy}{R_{\text{ref}}} \right)^{n-1},$$

where B_x and B_y are the horizontal and vertical transverse field components, B_1 is the dipole field component, and b_n and a_n are the "normal" and "skew" n-pole coefficients, also called the field harmonics, at a reference radius R_{ref}. The reference radius is usually chosen at two-thirds of the magnet free aperture.

Due to the symmetry of the magnet's cross-section, only normal multipole coefficients allowed by symmetry are expected to be non-zero (Brechna 1973; Mess et al. 1996; Russenschuck 2010). These so-called allowed multipole coefficients can be minimized by iterating on the coil cross-section parameters. In addition, the magnetic properties of coil and structural materials, and geometrical errors produce non-allowed field harmonics. For instance, a top/bottom asymmetry in a dipole magnet produces a skew quadrupole a_2, while a left/right asymmetry produces a normal quadrupole b_2. These unwanted harmonics can be minimized by selecting the appropriate materials and improving the precision of coil and structural components, tooling, and assembly procedures.

At the magnet design phase, two classes of field errors are distinguished: systematic and random errors. The systematic errors include geometrical errors, which originate from the imperfections of the coil and the iron yoke cross-sections, as well as by iron yoke saturation and coil magnetization. The random errors are mainly due to random variations of the coil geometrical parameters (inner and outer coil radii, coil pole angles, wedge geometry and position, etc.).

To achieve accelerator field quality, the coil and the yoke cross-sections and their relative position typically must have an accuracy better than ~0.1 mm including coil deformations under the Lorentz forces. The errors from Lorentz forces vary during magnet excitation, and their level depends on the rigidity of the coil and magnet mechanical structure. The minimization of these errors is one of the key parts of mechanical structure optimization.

The random errors are typically estimated by means of Monte Carlo simulations imposing a random displacement of the coil blocks. Since these displacements do not respect the magnet's symmetry, they produce a whole spectrum of field harmonics. Based on the random error analysis, fabrication tolerances for the main coil and structural components, tooling, and assembly process are formulated, which must be provided to achieve the required accelerator field quality.

The iron yoke is saturated when the level of field in the iron exceeds 2 T. The relative magnetic permeability of saturated iron is dramatically reduced depending

on the field level in each point of the yoke. As a result, the iron contribution is a non-linear function of the transport current. In a single-aperture magnet with a symmetrical iron yoke, the saturation effect is mainly observed in the magnet's main field B_1 (or magnet transfer function B_1/I) and in the normal sextupole b_3. The variation of sextupole field due to iron saturation is reduced by optimizing the iron inner and outer dimensions, and introducing special holes at appropriate places in the yoke. In a twin-aperture dipole, the central part of the yoke saturates before the outer parts, resulting in left/right asymmetries in the yoke contributions affecting the normal quadrupole b_2. The saturation effects in b_2 are of opposite sign in the two apertures. This effect is controlled by asymmetrical holes in the iron yoke and by choosing an inter-beam distance large enough to minimize these effects.

Three main components, which add to the field quality distortion from coil magnetization, are the persistent currents in the superconducting filaments; the eddy current between filaments within the strands; and the eddy currents between the strands of a cable, the so-called interstrand coupling currents. The field distortions produced by coil magnetization are most significant at low fields and become negligible at high fields. The field errors from coil magnetization change sign during current ramp up or down and, as a result, the main field and the allowed lower-order harmonics show ample hysteresis as a function of transport current and magnet excitation history.

The persistent currents in the filaments can be reduced by reducing their filament size. The eddy current component within the strands is controlled by the wire twist pitch, and the interstrand coupling currents depend on the interstrand resistance in the cable. The interstrand resistances should not be too large to allow current sharing among cable strands. If the cable's magnetic properties are uniform, only the main field and low-order allowed field harmonics (mainly b_3 and b_5) are disturbed. In the case of non-uniform magnetic properties, all lower-order harmonics will be affected.

1.2.3 Mechanical Design

The coil turns carrying a transport current in the magnetic field are exposed to electromagnetic (Lorentz) forces. The Lorentz force per unit length F/l of the conductor with current I in magnetic field B is

$$\vec{F}/_l = \vec{I} \times \vec{B}.$$

The force is directed perpendicularly to the current and field vectors. The value and distribution of forces inside the magnet coils, and the associated mechanical stress and deformations, depend on the magnet size and configuration, the value of the magnetic field, and the mechanical properties of the coil and the magnet structure. The analysis of mechanical forces, stresses, and deformations is a complex task, which is usually performed using finite element codes.

The Lorentz forces in superconducting accelerator magnets are very large (Mess et al. 1996; Ašner 1999). To stabilize the magnetic field characteristics in the operating field range and to reduce the probability of spontaneous quenches, it is necessary to ensure the mechanical stability of turns in the coil. Mechanical stability is achieved by applying a preload to the coil during magnet assembly and by supporting the compressed coil during operation with a rigid support structure. The required minimum preload value is determined by the magnet design, the level of the operating field, and the thermal contraction and mechanical rigidity of the structural materials. The allowed coil pre-stress is limited by the maximum stress that the coil can sustain before the superconductor starts degrading or before insulation damage. The preload applied to the magnet coils at room temperature has to be sufficient to compensate for the preload decrease due to coil creep after magnet assembly, differences in thermal contraction of the coil and structure, and coil deformations under Lorentz forces during magnet excitation.

The horizontal component of the Lorentz force bends the coil horizontally with a maximum displacement at the magnet mid-plane. This bending leads to additional coil stress and to a coil deformation that generates field distortions. The coil support against the horizontal component of the Lorentz force is provided by a special stiff support structure placed between the coil and the iron yoke. This structure is optimized to limit the horizontal coil deflections. To increase the field enhancement from the iron yoke, however, it is placed rather close to the coil, which limits the thickness and, thus, rigidity of the support structure. To compensate for this, the yoke and strong metallic shell outside the yoke or the helium vessel shell are also used as part of the coil support system.

The axial component of the Lorentz force stretches the coil axially, increasing stresses and turn displacements in the coil ends. To minimize these effects, it is essential to provide a stiff support (and even some initial axial preload to compensate for different thermal contraction of the magnet coils and mechanical structure) against the axial component of the Lorentz force using thick stainless-steel end plates welded to the shell or connected by thick axial rods.

1.2.4 Operation Temperature, Fields and Margins

Superconducting magnets are operated at temperatures well below the superconductor's critical temperature. Liquid helium, which has a boiling temperature of around 4.22 K at atmospheric pressure (Weisend 1998), is usually used for this purpose. At temperatures below 2.17 K, called the lambda point, liquid helium turns into a superfluid due to a phase transition. The superfluid phase has extremely high thermal conductivity and extremely low viscosity. This combination of properties is beneficial for the cooling of superconducting magnets as it allows the superfluid helium to penetrate into a porous coil and magnet structure, and to transfer heat from the magnet to a heat sink in a stagnant liquid superfluid helium bath.

The superconductor critical current density is a function of its temperature and the applied magnetic field. Figure 1.2 shows the dependence of the conductor critical

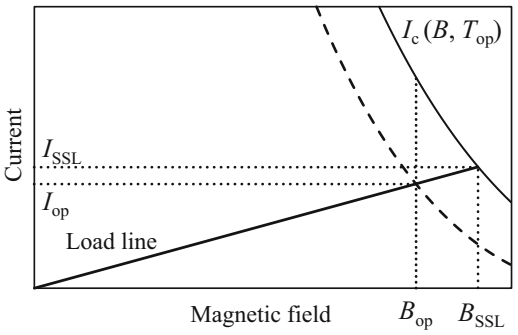

Fig. 1.2 Conductor I_c vs. magnetic field B and magnet load line

current, defined as the maximum transport current carried through the superconductor area vs. the magnetic field for a given operating temperature T_{op}. The magnet load line describing the dependence of the magnetic field in the coil and the magnet current is also shown. The intersection of these two functions defines the magnet's ultimate parameters such as the maximum field B_{SSL} and the maximum current I_{SSL}, also known as the magnet short sample limits (SSL).

To ensure stable performance, superconducting magnets operate at currents below the conductor critical current with some margin. Important magnet operation margins include the margin along the load line, defined as the ratio of the operation current to the magnet short sample limit, $i = I_{op}/I_{SSL}$, and the critical current margin, defined as the ratio of the operation current to the conductor critical current at B_{op} and T_{op}

$$i = I_{op}/I_c\left(B_{op}, T_{op}\right).$$

The magnet temperature margin ΔT, associated with the critical current margin, is defined as the difference between the operation temperature T_{op} and the current sharing temperature T_{cs} at which the operation current is equal to the critical current. Note that the critical current margin and the temperature margin are different for each turn, due to the field and related critical current variations inside the coil.

1.2.5 Magnet Thermal Stabilization

Superconducting magnet coils are exposed to a variety of disturbances such as conductor displacements during excitation, epoxy cracking, AC losses, splice heating, beam-induced heat deposition, fluctuations of the helium temperature in the cryogenic system, etc. These disturbances may raise the coil temperature above the superconductor critical temperature T_c, as the transport current is expelled into the low-resistivity matrix. The main goal of coil thermal stabilization is ensuring

its ability to stay superconducting, or to recover superconductivity after a disturbance.

To achieve complete magnet thermal stability with respect to any perturbations, the cross-section of the normal stabilizer has to be rather large and well-cooled (Brechna 1973; Weisend 1998). Considerations related to cost and performance optimization, however, require reducing the stabilizer cross-section in superconducting accelerator magnets to a minimum, as dictated by the internal stability of the composite wires to flux jumps and by quench protection. In this case, complete magnet stability is not provided. Some improvement of magnet stability can be achieved by limiting the conductor motion in a coil by applying coil preload, by coil impregnation (e.g., with epoxy or other suitable agents), and by reducing friction on various conductor surfaces inside a magnet.

The perturbation spectrum is usually not known for superconducting magnets. In this case, magnet pre-conditioning plays an important role for releasing large perturbations accumulated during magnet fabrication. In early experiments with superconducting magnets it was found that the magnet maximum current gradually increases in consequent quenches. This process is known as magnet training. After a limited number of quenches a magnet often reaches a stable plateau. If the magnet quench current at the plateau is lower than the magnet short sample limit, it indicates a magnet current degradation. Magnets usually remember their training after warming-up and cooling-down cycles, or show only a very short retraining. This memory is extremely important for accelerator magnets, which are installed and connected in series in large-scale accelerators.

Despite the disadvantages associated with possible instabilities and training, partially stabilized accelerator magnets provide the highest engineering current densities in the coils and, thus, enable the most compact magnets and the highest fields at the lowest cost.

In the case of AC losses, radiation-induced heat deposition, splice heating, and other steady or pulsed heat losses, the perturbation power is known and the coil peak temperature T_{coil} is defined by

$$T_{\mathrm{coil}} - T_{\mathrm{op}} = \frac{q_{\mathrm{v}} A}{hP}$$

for a steady heat deposition, or

$$W = \int_{T_{\mathrm{op}}}^{T_{\mathrm{coil}}} C_{\mathrm{p}}(T)\mathrm{d}T$$

for a pulsed heat deposition, where q_{v} is the average volumetric heat load, W is the heat pulse energy, A is the cable cross-sectional area, h is the heat transfer coefficient, P is the conductor cooling perimeter, and T_{op} is the operating temperature. To prevent magnet quenches, the temperature everywhere in the magnet coil should be kept below T_{c}. Magnet stability is ensured by choosing an appropriate temperature margin and coil cooling conditions.

1.2.6 Quench Protection

The stored energy in superconducting accelerator magnets is large. In the case of a quench, a large portion of this stored energy is typically dissipated in the relatively small coil volume and, thus, the coil is heated to quite high temperatures, which may damage or even destroy the coil. Hence, the magnet and conductor design and the protection system parameters have to be optimized to provide for reliable magnet protection during a quench and to limit the coil temperature, thermal stress, and voltages within acceptable values (Wilson 1983; Mess et al. 1996; Iwasa 2009).

The peak quench temperature $T_{\max}$ is usually estimated using an adiabatic approach by equating the Joule heat in the coil during the quench to the increase of the coil enthalpy

$$\int_0^\infty I(t)^2 \mathrm{d}t = \lambda S^2 \int_{T_\mathrm{q}}^{T_{\max}} \frac{C(T)}{\rho(B,T)} \mathrm{d}T$$

where $I(t)$ is the current decay after a quench, T_q is the conductor quench temperature, S is the total conductor cross-section, λ is the stabilizer fraction in the conductor cross-section, $C(T)$ is the average conductor specific heat, and $\rho(B,T)$ is the conductor normal resistivity. For a given value of the so-called quench integral usually measured in million ampere squared seconds (MIITS, 10^6 $\mathrm{A}^2\,\mathrm{s}$), $T_{\max}$ can be minimized by reducing the matrix resistivity, or by increasing the conductor cross-section and the average specific heat. The value of the total quench integral is controlled by the quench detection and validation time, the protection circuit response, and the current decay time.

If the quench propagates rapidly inside a magnet, the stored energy can be practically uniformly dissipated in the magnet coil. The magnet will be self-protected if the enthalpy of the quenched part of the coil is sufficient to keep the magnet's maximum temperature below the acceptable level, usually 300–400 K. Quench protection of large accelerator magnets requires a special protection system based either on traditional resistive quench heaters or on the recently developed Coupling Loss Induced Quench (CLIQ) system (Ravaioli 2015). Both approaches provide a rapid quench of a large coil volume, sufficient to absorb the magnet storage energy without coil overheating.

Protection heaters are usually made of thin stainless-steel strips, which are placed on the coil surface. Since the heaters are electrically insulated from the coil, the heater electrical insulation introduces a thermal barrier. As a result, there is a delay between heater excitation and the coil quench. The heaters and their integration into the coil structure are optimized to reduce this delay. In the CLIQ system, capacitor banks are discharged over parts of the coil, inducing eddy currents that quench the coil quasi-instantaneously.

The natural quench propagation in the coil, as well as the heat transfer between the quenched coil and the magnet support structure, increases the effective magnet volume involved in the energy dissipation and allows the dissipation of some

fraction of the stored energy outside the coil. It reduces the hot-spot temperature and the temperature under the quench heaters. In some cases, the magnet current decay is fast enough that eddy currents induced in the conductor may also quench superconducting parts of the coil. This phenomenon, known as the "quench-back" effect, evidently helps to reduce the peak coil quench temperature. Using a protective heating system also helps to provide a more balanced temperature and voltage distributions, and reduce the thermal and electrical stresses in the coil.

1.3 Nb-Ti Accelerator Magnets and Technologies

The work on Nb-Ti superconducting magnets for accelerators started in the late 1960s (Prodell 1968) and culminated from the 1980s to the 2000s in the construction of a series of large superconducting accelerators in the USA and in Europe (Edwards 1985; Meinke 1991; Anerella et al. 2003; Evans and Bryant 2008). These powerful superconducting accelerators have enabled several fundamental discoveries, including the charm and top quarks, the tau lepton, the gluon, the Z and W bosons and, most recently, the Higgs boson, which have shaped and confirmed our understanding of the particle physics Standard Model.

1.3.1 Nb-Ti Composite Wire

The superconducting Nb-Ti alloy, discovered in the 1960s, is the most successful practical superconductor. Since the 1970s, it has been the workhorse for superconducting accelerator magnets, thanks to its ductility, high current carrying capability, and the successful industrialization of the composite wires based on this material. Its critical temperature at zero magnetic field, T_{c0}, is 9.8 K; and the upper critical magnetic field at zero temperature, B_{c20}, is 14.5 T.

The Nb-Ti composite wires are manufactured by a co-drawing process with intermediate heat treatments to achieve an optimal critical current density. The final annealing provides a high residual resistivity ratio (RRR) for the copper stabilizer. A thin Nb barrier separates the Nb-Ti alloy from the copper to avoid the formation of a brittle CuTi intermetallic composite during the high-temperature extrusion and the annealing heat treatments.

Diameters of practical wires are in the range 0.1–3 mm, and piece lengths are of a few kilometers. The number of filaments in a wire may reach ~10^5, and the filament diameter is typically 5–20 μm (the practical low limit is ~1–2 μm). The filament size is determined mainly by the stability criteria and by hysteresis magnetization or AC loss requirements. The critical current density in a superconductor at 5 T and 4.2 K in Nb-Ti composite wires used in accelerator magnets increased from ~1.5 kA/mm^2 to more than 3 kA/mm^2 today. The typical RRR values of the copper matrix are in the range 50–200.

1.3.2 Nb-Ti Accelerator Magnet Designs and Technologies

The first large superconducting accelerator based on Nb-Ti magnets was the Tevatron (1983–2011) at the Fermi National Accelerator Laboratory (FNAL, USA). It was followed by the Hadron Elektron Ringanlage (HERA, 1991–2007) at the Deutsches Elektronen-Synchroton (DESY, Germany), the Relativistic Heavy Ion Collider (RHIC, since 2000) at Brookhaven National Laboratory (BNL, USA), and the Large Hadron Collider (LHC, since 2008) at the European Organization for Nuclear Research (CERN).

Cross-sections of the Nb-Ti dipole coils used in arc dipoles in these projects are shown in Fig. 1.3. Coil and cable parameters are summarized in Table 1.1.

Figure 1.4 shows cross-sections of the dipole magnets in their cryostats, so-called cryo-magnets. The main arc dipole parameters are shown in Table 1.2.

These figures and the data in Tables 1.1 and 1.2 show the main tendencies in the evolution of the coil and magnet designs.

The Tevatron was the highest-energy hadron collider until its shutdown in 2011. It had a circumference of ~6.9 km and consisted of 774 dipoles and 240 quadrupoles, as well as more than 200 corrector spool pieces. A key element for the success of the Tevatron was the use of superconducting dipoles wound from Rutherford cables as two-layer shell-type coils. The mechanical structure was based on precise stainless-steel collars to apply coil azimuthal pre-stress and radial support. To ensure protection, quench heaters were used to accelerate the normal zone propagation in the coil during a quench. Tevatron magnets also featured a compact cryostat design with a warm iron yoke. This approach led to some problems with the centering and alignment of the collared coils inside the warm iron yoke, and to quite large heat

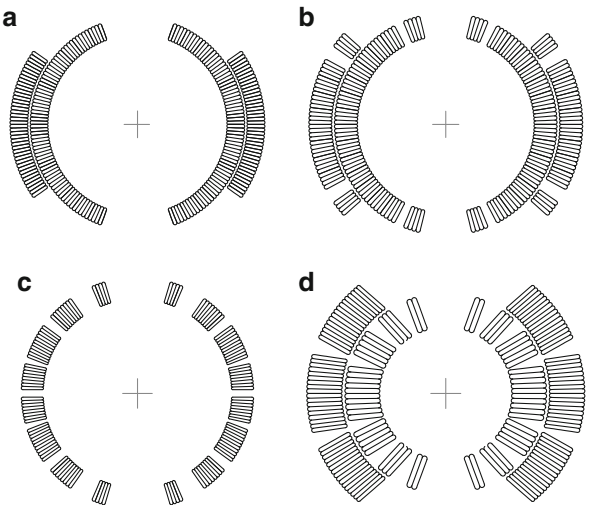

Fig. 1.3 Magnet coil cross-sections: (**a**) Tevatron; (**b**) HERA; (**c**) RHIC; (**d**) LHC

Table 1.1 Coil and cable parameters

	Tevatron	HERA	RHIC	LHC
Coil aperture (mm)	76	75	80	56
Number of turns	35/21[a]	32/20[a]	31	15/25[a]
Strand diameter (mm)	0.68	0.84	0.65	1.065/0.825[a]
Superconducting filament diameter (μm)	9	14	6	7/6[a]
Cu:Superconductor ratio	1.8	1.8	2.25	1.65/1.95[a]
Number of strands in cable	23	24	30	28/36[a]
Cable thickness (mm)	1.26	1.48	1.16	1.9/1.48[a]
Cable width (mm)	7.77	10.0	9.7	15.1/15.1[a]

[a] Inner/outer layers

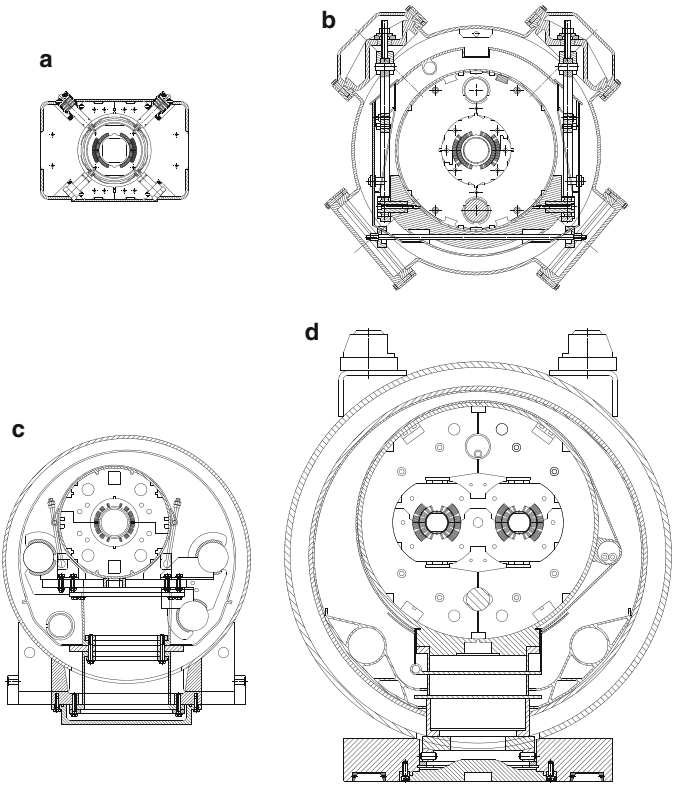

Fig. 1.4 Accelerator dipole cross-sections: (**a**) Tevatron; (**b**) HERA; (**c**) RHIC; (**d**) LHC

leaks to the helium vessel through the short plastic supports. The alignment problem was solved by the invention of spring-loaded smart bolts. The high level of heat leaks through the support system did not, however, allow the achievement of the design operation temperature and, thus, the target beam energy of 1 TeV. Despite these small hick-ups, the design and production of the Tevatron superconducting magnets opened the era of large superconducting accelerators.

Table 1.2 Arc dipole parameters

	Tevatron	HERA	RHIC	LHC
Aperture (mm)	76	75	80	56
Magnetic length (m)	6.1	8.8	9.45	14.3
Nominal bore field (T)	4.3	5.3	3.5	8.3
Nominal current (kA)	4.3	5.7	5.1	11.9
Stored energy at I_{nom} (MJ)	0.30	0.94	0.35	6.93
Operation temperature (K)	4.6	4.5	4.3–4.6	1.9

The next large superconducting accelerator, HERA, comprised a 30 GeV electron storage ring (SR) with conventional electromagnets and a 820 GeV superconducting proton SR. The 820 GeV ring had a circumference of ~6.3 km and consisted of 422 main dipoles and ~225 main quadrupoles, along with approximately the same number of superconducting correcting elements. The dipole magnets of the proton ring were developed at DESY, while the quadrupole magnets were developed at the Commissariat à l'Energie Atomique at Saclay (CEA/Saclay) near Paris, France. HERA dipoles, designed to produce 4.7 T at 4.6 K, subsequently operated at 5.5 T by reducing the magnet operation temperature below 4 K. The HERA dipoles used thick, free-standing aluminum collars and a cold iron yoke. The cold iron yoke design selected, greatly simplified the collared coil alignment inside the yoke and reduced heat leaks to the magnet cold mass by using long plastic suspensions and better thermal insulation at the expense of a much larger cold mass. The HERA arc dipoles were manufactured in industry, which required a significant improvement of magnet technology, technology transfer to industry, and the provision of reliable quality control throughout magnet production. This brave and cost-saving step was adopted later by the next large-accelerator projects.

The RHIC is designed to collide beams of nuclei as heavy as gold, accelerated in two identical SRs to energies between 7 GeV and 100 GeV per beam and per unit of atomic mass. RHIC beams are guided by 3.5 T dipole magnets. Each of the two separate superconductor SRs is ~3.8 km in circumference and they intersect at six points. Each ring consists of ~1740 superconducting magnets, including 264 arc dipoles and 276 arc quadrupoles. An important goal of the RHIC magnet design was to minimize magnet cost, which was achieved by using a single-layer shell-type coil design, thin plastic coil–yoke spacers instead of expensive metallic collars, and a cold iron yoke close to the coil, which adds ~30% to the field in the bore. The coils, surrounded by glass-reinforced phenolic spacers, are preloaded and supported by a horizontally split iron yoke and a stainless-steel skin. The magnet cold mass is installed inside a vacuum vessel on Superconducting Super Collider (SSC)-type plastic support posts, that were used later in the LHC magnets. Several improvements in the dipole design included the optimization of the field quality in operation field range with a saturated iron yoke, high-J_c superconducting strand with 5–6 μm filaments, and 10 mm wide Rutherford cable. As with HERA, the RHIC dipoles were produced by industry, including systematic warm magnetic measurements for quality control.

The LHC is the largest superconducting proton–proton collider in the world, with an SR of ~27 km in circumference and the highest operation dipole field of 8.33 T. It is located in an underground tunnel previously constructed and used for the Large Electron–Positron Collider (LEP). The ring is filled with 1276 superconducting dipoles and ~425 quadrupoles. The dipole magnets were developed at CERN, while the quadrupole magnets were developed at CEA/Saclay. The dipole design is based on two-layer shell-type graded coils with two 15 mm wide Rutherford cables in the inner and outer layers. The coils are preloaded with thick stainless-steel collars and supported by a vertically split cold iron yoke. The LHC dipoles adopted for the first time a two-in-one design concept in which two apertures with opposite field directions are placed inside a common collar and iron yoke. The LHC magnets use high-performance composite wires made of high homogeneity Nb-Ti alloy and are cooled by superfluid helium at 1.9 K, which further enhances the performance of the Nb-Ti conductor and, thus, increases the magnet operating field. As with the HERA and RHIC magnets, all of the LHC dipoles were produced in industry. The production of the LHC dipoles was shared by three European companies.

In parallel with the development and construction of superconducting magnets for HERA, from the 1980s until the early 1990s, Nb-Ti magnets were developed for the 3 TeV Uskoritel'no Nakopitel'nyj Kompleks (UNK) (Accelerator and Storage Complex) in Protvino, near Moscow, Russia, at the Institute for High Energy Physics (Ageyev et al. 1980), and for the 40 TeV SSC near Waxahachie, Texas, (Jackson 1986). Both dipole designs were similar to the HERA dipole. The UNK dipoles had an aperture of 80 mm and were designed to operate at a nominal field of 5 T at 4.5 K. The magnets used circular stainless-steel collars. The magnet cold masses were suspended inside the vacuum vessel using long Ti-alloy rods. The SSC dipoles had an aperture of 50 mm (the initial design had an aperture of 40 mm) and a nominal operating field of 6.6 T at 4.3 K. Special plastic posts were developed for the SSC magnets to support the cold masses inside the vacuum vessel. Although a series of short dipole models and full-scale prototypes have been produced and successfully tested in the framework of both projects, these two projects were terminated in the middle of the 1990s.

1.4 Next Generation of Superconducting Accelerator Magnets

A field of ~10 T is considered to be the practical limit for Nb-Ti accelerator magnets. As shown above, using magnets with a higher field is the most efficient way to achieve higher collision energies in those accelerators. To produce higher fields, new superconducting materials with better properties are needed. The only practical material that is readily available on an industrial scale is an intermetallic Nb_3Sn compound, which belongs to the A15 crystallographic family.

1.4.1 Nb_3Sn Composite Wires

The superconducting properties of the Nb_3Sn compound, as for the Nb-Ti alloy, were also discovered in the 1960s. The work on Nb_3Sn accelerator magnets started practically immediately in the late 1960s, motivated by the better critical parameters of Nb_3Sn. The critical temperature T_{c0} of Nb_3Sn is 18 K and the upper critical magnetic field B_{c20} is 28 T.

Nb_3Sn composite wires are currently produced using three main methods: bronze, internal tin (IT), and powder-in-tube (PIT) (Rogalla and Kes 2012). The bronze process is based on a large number of Nb filaments dispersed in a Sn-rich bronze matrix. The bronze route provides the smallest filament size (~2–3 μm), but has a relatively low critical current density due to the limited Sn content in bronze available for reaction to Nb_3Sn. The IT process is based on assembling a large number of Nb filaments and pure Sn or Sn-alloy rods in a copper matrix. Restacking of assemblies allows the reduction of the final sub-element size. Due to the optimal amount of Sn, this process provides the highest critical current density, but limits the minimum sub-element size currently achievable in the final wire to ~40–50 μm. The PIT process is based on stacking thick-wall Nb tubes, filled with fine $NbSn_2$ powder in a high-purity Cu matrix. This method provides a reasonable combination of small filament size (<50 μm) and high critical current density comparable with the IT process. The cost of PIT wire is, however, still considerably higher than the cost of IT wire. In all of these methods, the Nb_3Sn phase is produced during a final multi-stage high-temperature heat treatment with a maximum temperature ~650–700 °C for 50–100 h.

As the accelerator construction costs are driven by the ring circumference, superconducting magnets for particle accelerators rely on the highest possible current density to minimize the coil volume and magnet cost. Thus, IT and PIT composite wires are the most appropriate for use in high field accelerator magnets. The highest value of the critical current density at 12 T and 4.2 K in state-of-the-art Nb_3Sn composite wires developed for use in accelerator magnets exceeds 3 kA/mm^2.

Nb_3Sn composite wires are compatible with the Rutherford cable design and technologies, making the Rutherford cable a primary option for use in Nb_3Sn accelerator magnets. Due to the more delicate structure and mechanical properties of the Nb-Sn precursor, however, forming the compact keystoned cable cross-section without degrading the strand critical current is challenging. This problem, as well as strand fusing in cables during high-temperature heat treatment of coils under pressure, requires special attention and optimization.

1.4.2 Design Issues of Nb_3Sn Accelerator Magnets

All the abovementioned accelerators with Nb-Ti magnets have been built based on the shell-type (also known as cos-theta) designs. This design is also suitable for use

with the Nb_3Sn superconductor. In this design, keystoned Rutherford cables are wound in blocks, which are spaced with wedges, around a circular bore. The number of cables in each block and the dimensions of the wedges are selected such that field errors and the conductor peak field to bore field ratio are minimized. Thanks to the Roman arch principle, no internal support structure is required in the cos-theta structure. Consequently, no valuable real estate inside the aperture is lost.

An alternative, the block coil design, is based on racetrack coils with a vertical turn position and flared ends. A special support structure is usually required in high field dipoles to support the pole blocks and flared ends. In the late 1990s, a common-coil approach, first proposed in the early 1980s for low field Nb-Ti magnets, was considered for high field dipole magnets. The common-coil design is a twin-aperture version of the block-type dipole with vertically positioned apertures. In this design flat racetrack coils are shared between the two apertures. This coil arrangement and simple coil geometry provide some technological advantages. In particular, the coil radii in this design are defined by the distance between apertures rather than by aperture size, making it suitable for the winding of brittle conductors such as Nb_3Sn.

In the late 1990s, it was postulated that the block-type coil design is better suited for high field Nb_3Sn magnets than the cos-theta design (Sutter and Strauss 2000). This statement started to be intensively disputed within the accelerator magnet community. The main debate points are the coil winding issues (racetrack coils with flared ends vs. coils wound around a cylinder); the relative position of high field and high stress areas (cos-theta magnets have the highest stress in the coil mid-plane where the field level is also large whereas block coils have the largest stress level in the low field parts); the possibility of using wider cables in block coils than is feasible in the cos-theta coils, allowing for smaller inductance and larger operating current; and the amount of conductor required to achieve the same field level.

All three different coil types based on Nb_3Sn Rutherford cables have been designed, manufactured, and tested. In the following chapters, they are thoroughly described and discussed. The question of which of these options is best suited for the hadron collider continues to be passionately debated within the scientific community.

1.4.3 Nb_3Sn Magnet Technology

The fabrication of Nb_3Sn magnets is a complicated process due to the delicate processing, brittleness, and stress/strain sensitivity of Nb_3Sn composite wires and cables. It imposes serious limitations upon the use of reacted Nb_3Sn conductors for coil winding (react-and-wind technology). To overcome the limitations of working with brittle conductors, the so-called wind-and-react technology was introduced. In this approach, a coil is wound with a ductile conductor made of the Nb-Sn precursors. Afterwards, the coil is reacted at temperatures of up to 650–700 °C for several days to form the brittle superconducting Nb_3Sn phase. The high temperature during the coil reaction excludes the use of organic materials for cable and coil insulation as well as for various coil components.

The phase transition during the formation of the Nb_3Sn leads to a radial and azimuthal coil expansion after reaction. In the axial direction, this effect is compensated for by the coil contraction due to a release of stress accumulated in the strand matrix during cable fabrication. In practice, the exact dimensional changes of the coil depend on the cable compaction and on the insulation used. No empirical fitting-law for the exact prediction of the dimensional change of the conductor during reaction has yet been established. It is determined for each cable and coil design empirically in trial coil cross-sections. The empirical data for each specific project need to be established and considered during coil assembly and preloading.

The Nb_3Sn conductor, if exposed to stress/strain, shows a degradation of the critical current density. Depending on the stress/strain value the degradation is reversible or irreversible. Stress/strain analysis and optimization of the magnet assembly process are important parts of magnet design and technology development. For example, applying excessive pre-stress during magnet assembly, to compensate for pre-stress lost while the magnet cools down to the operating temperature, could cause irreversible degradation of the Nb_3Sn coils. The engineering of mechanical structures using materials with different thermal contraction coefficients to avoid pre-stress loss, or even to achieve pre-stress increase, is important for exploring the potential of Nb_3Sn accelerator magnets.

Good field quality, as discussed above, is mandatory in accelerator magnets. All the major components—geometric, iron saturation, and coil magnetization effects—require special attention in Nb_3Sn magnets. Geometric field errors, controlled by the position of the coil turns, are impacted by the turn expansion and possible displacements during coil reaction as well as by turn motion under large Lorentz forces. The iron saturation effects are larger due to the larger field level and larger field variations in the yoke. Persistent current field errors are larger due to the large superconductor filament sizes and higher critical current density in Nb_3Sn filaments. In addition, the field errors related to the interstrand eddy currents in cable can also be very large due to strand fusing during coil reaction.

Lastly, due to the large scale of future circular hadron colliders, the cost-optimization of Nb_3Sn magnets becomes of high importance.

1.4.4 Magnet Performance Test

Sophisticated analysis tools, available at the present time to magnet designers, allow for accurate magnet analysis (magnetic, mechanical, thermal) and the exact definition of the magnet target parameters based on the properties of materials and the operating conditions. Many uncertainties in material properties as well as variations of technological procedures inevitably, however, affect magnet performance. As a result, the difference between the real magnet performance and the magnet target parameters can be significant. Therefore, detailed material characterization, quality control during all production steps, and final comprehensive magnet tests are important components of a successful magnet production process development.

Before performing the final magnet tests at the nominal operating conditions, tests at ambient temperature are typically conducted. The final magnet tests are performed at the nominal operation conditions. Both magnet production and final cold tests not only provide the final performance parameters but also their reproducibility from magnet to magnet in large series. During the research and development phase, these tests provide very important feedback for the optimization of magnet design, technology, and performance.

The main objectives of the magnet cold tests are the examination of all magnet design parameters including the quench performance study, magnetic measurements, quench protection studies, and measurements of magnet mechanical properties. The list of tests, their sequence, and conditions are defined in a magnet test plan, which is prepared for each magnet. This plan consists of the standard test procedures common for all magnets of a given series, as well as some specific tests for each magnet.

To measure the magnet performance parameters, each magnet is equipped with appropriate instrumentation. Some elements of the instrumentation (voltage taps, strain and temperature gauges, heaters, etc.) are implemented during magnet assembly, whereas the others are placed inside the magnet bore (quench antenna coils, and Hall probes or rotating coils for magnetic measurements) or on the magnet skin and end plates (strain gauges, bullet gauges, thermometers).

The following examples illustrate the importance of magnet final tests and the important feedback that they provide. Quenches below the magnet short sample limit point to possible energy depositions in the magnet coil due to turn frictional motions under the Lorentz force, heat dissipation from losses in the cable, or non-uniform current distribution among cable strands. The non-uniform distribution of the transport current in the cable is also visible in longitudinal oscillations of the field harmonics. The current imbalances may be caused by non-uniform properties of strands in the cable, non-uniform solder joints connecting the coils to the current leads, or large eddy current loops formed by small local interstrand resistance.

Other effects that are observed during cold tests of superconducting accelerator magnets and the way they are being addressed during the magnet development phase will be presented and discussed in the next chapters of this book.

References

Ageyev AI, Balbekov VI, Dmitrevsky YP et al (1980) The IHEP accelerating and storage complex (UNK) status report. In: Newman WS (ed) 11th international conference on high-energy accelerators, Genè, 7–11 July 1980. Springer Basel AG, Basel, p 60

Anerella M, Cottingham J, Cozzolino J et al (2003) The RHIC magnet system. Nucl Instrum Meth A 499:280–315

Ašner FM (1999) High field superconducting magnets. Oxford University Press, Oxford

Brechna H (1973) Superconducting magnet systems. Springer, Berlin/Heidelberg

Edwards HT (1985) The Tevatron energy doubler: a superconducting accelerator. Ann Rev Nucl Part Sci 35(1):605–660. https://doi.org/10.1146/annurev.nucl.35.1.605

Evans L, Bryant P (2008) LHC machine. J Instrum 3(8):S08001. https://doi.org/10.1088/1748-0221/3/08/s08001
Gallagher-Daggit G (1973) Superconductor cables for pulsed dipole magnets. Technical report, Rutherford High Energy Laboratory Memorandum, No. RHEL/M/A25, Chilton, Didcot
Iwasa Y (2009) Case studies in superconducting magnets: Design and operational issues. Springer, New York
Jackson JD (1986) Conceptual design of the superconducting super collider. SSC-SR-2020, SSC Central Design Group, Berkeley
Meinke R (1991) Superconducting magnet system for HERA. IEEE Trans Magn 27(2):1728–1734. https://doi.org/10.1109/20.133525
Mess K-H, Wolff S, Schmüser P (1996) Superconducting accelerator magnets. World Scientific, Singapore
Prodell AG (ed) (1968) BNL summer study. Brookhaven National Laboratory, Upton. http://www.bnl.gov/magnets/Staff/Gupta/Summer1968/contents.html
Ravaioli E (2015) CLIQ. A new quench protection technology for superconducting magnets. PhD Thesis, University of Twente
Rogalla H, Kes PH (eds) (2012) 100 years of superconductivity. CRC Press, Boca Raton
Russenschuck S (2010) Field computation for accelerator magnets. Wiley-VCH, Weinheim
Sutter DF, Strauss BP (2000) Next generation high energy physics colliders: technical challenges and prospects. IEEE Trans Appl Supercond 10(1):33–43. https://doi.org/10.1109/77.828171
Warnes WH, Larbalestier DC (1987) Determination of the average critical current from measurements of the extended resistive transition. IEEE Trans Magn 23(2):1183–1187. https://doi.org/10.1109/tmag.1987.1065081
Weisend JG II (ed) (1998) Handbook of cryogenic engineering. Taylor & Francis, Reading
Wilson MN (1983) Superconducting magnets. Oxford University Press, New York
Wilson MN (2012) 100 years of superconductivity and 50 years of superconducting magnets. IEEE Trans Appl Supercond 22(3):3800212. https://doi.org/10.1109/tasc.2011.2174628
Wolski A (2014) Beam dynamics in high energy particle accelerators. Imperial College Press, London